analytical chemistry

pubs.acs.org/ac Article

Regenerative Flexible Upconversion-Luminescence Biosensor for Visual Detection of Diethylstilbestrol Based on Smartphone Imaging

Jizhong Wu, Waqas Ahmad, Qin Ouyang,* Jingui Zhang, Mingming Zhang, and Quansheng Chen*

Cite This: *Anal. Chem.* 2021, 93, 15667−15676 Read Online

ACCESS | Metrics & More | Article Recommendations | Supporting Information

ABSTRACT: Diethylstilbestrol (DES), an endocrine disrupting chemical, has been linked to serious health problems in humans. In this work, a regenerative flexible upconversion-fluorescence biosensor was designed for the detection of DES in foodstuffs and environmental samples. Herein, amino-functionalized upconversion nanoparticles (UCNPs) were synthesized and immobilized on the surface of a flexible polydimethylsiloxane substrate, which was further modified with complementary DNA and dabcyl-labeled DES aptamer. The fluorescence resonance energy transfer (FRET) system was established for DES detection between dabcyl and UCNPs as the acceptor and donor pairs, respectively, which resulted in the quenching of the upconversion luminescence intensity. In the presence of a target, the FRET system was destroyed and upconversion fluorescence was restored due to the stronger affinity of the aptamer toward DES. The designed biosensor was also implemented in a dual-mode signal readout based on images from a smartphone and spectra from a spectrometer. Under the optimized experimental conditions, good linear relationships were achieved based on imaging ($y = 53.055x + 36.175$, $R^2 = 0.9851$) and spectral data ($y = 1.1582x + 1.9561$, $R^2 = 0.9897$). The designed biosensor revealed great practicability with a spiked recovery rate of 77.91−97.95% for DES detection in real environment and foodstuff samples. Furthermore, the proposed biosensor was regenerated seven times with an accuracy threshold of 80% demonstrating its durability and reusability. Thus, this biosensor is expected to be applied to point-of-care and on-site detection based on the developed portable smartphone device and android application.

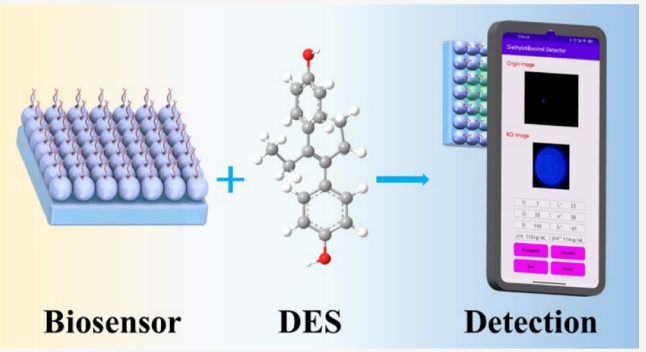

1. INTRODUCTION

The potential health threat posed by endocrine disrupting chemicals (EDCs) present in our environment, cosmetics, foodstuff, and medications has received considerable interest due to its possible interference with the normal body functions such as hormone biosynthesis and metabolism.[1] Diethylstilbestrol (DES), an estrogen like EDC compound, was initially used to prevent premature delivery, miscarriage, and pregnancy complications and used afterward as a veterinary drug to promote animal growth.[2,3] However, DES, as an exogenous estrogen, imitates endogenous estrogen[4] and has the potential to cause a detrimental effect on human health such as adverse reproductive barriers,[5] long-term changes in sexual behavior,[6] cervical intraepithelial neoplasia,[7] and so forth. United States, China, Europe, and some other countries have instituted strict restrictions on the use of DES in food. Therefore, it is important to design new and reliable strategies for fast and sensitive detection of DES to ensure public safety. A number of methods for DES detection methods have shown promise such as solid-phase extraction coupled high-performance liquid chromatography,[8] electrochemiluminescence,[9] molecularly imprinted polymer-coated quantum dots,[10] photoelectrochemical immunosensor,[11] and so forth. Despite the sensitivity of some of these methods, their implementation is hampered by the lack of professional operation skills, expensive instruments, and high test costs. As a result, it is critical to develop an affordable and convenient sensor as well as portable equipment for DES detection.

To comply with the preceding criteria, long-term storage, portable, and reusable solid-phase biosensors should be utilized. Immobilizing nanoparticles, biomolecules, and compounds on solid substrates allows for the construction of a portable reaction platform that avoids bioreceptor denaturation and nanoparticle agglomeration.[12] Solid-phase sensors have recently been used in a variety of fields due to their appealing properties, as evidenced by their use in disease diagnosis,[13] noncontact thermometry,[14] hazardous compound determination,[15] and so forth. Flexible substrates, among solid-

Received: August 5, 2021
Accepted: November 9, 2021
Published: November 17, 2021

https://doi.org/10.1021/acs.analchem.1c03325
Anal. Chem. 2021, 93, 15667−15676

Scheme 1. Schematic Diagram of Fabrication, Detection, and Regeneration of a Flexible Biosensor

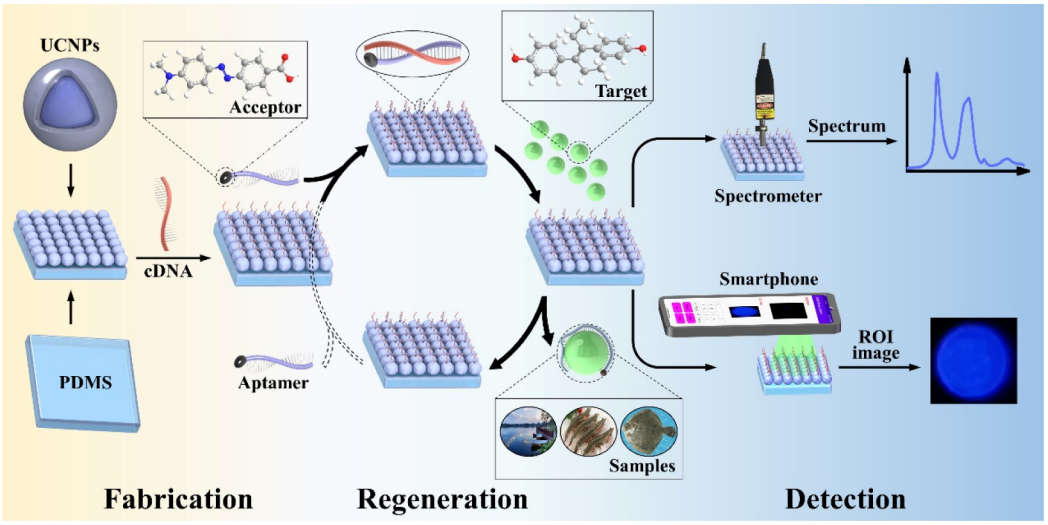

phase sensor substrates, have the highest potential for designing portable and cost-effective biosensors due to their useful deformability and simplicity of segmentation.[16] In addition, the bioreceptor of the biosensor is the key element to accurately identify the object. The aptamers purified in vitro by systematic evolution of ligands by exponential enrichment (SELEX) as bioreceptors have demonstrated affinity similar to that of antibodies with higher stability, flexibility to modification, and lower cost.[17] Among the aptamers used for DES detection in the literature include a 17β-estradiol sequence rather than DES which may be due to the fact that its specific sequence had not been explored at that time.[18,19] A recent magnetic-based SELEX strategy looking for an aptamer specific to DES[20] possibly paved the way for developing a flexible aptasensor. Moreover, to design an economical flexible biosensor, the fluorescent material is regarded as a strong candidate.

Rare-earth doped upconversion nanoparticles (UCNPs) are fascinating fluorescent nanomaterials with anti-Stokes luminescence properties. UCNPs convert low-energy near-infrared light (808 or 980 nm) into high-energy visible light to achieve upconversion luminescence (UL) via two-photon or multiphoton mechanism.[21] Thus, UCNPs have a number of conspicuous advantages over traditional downconversion fluorescent materials, including longer fluorescence lifetime, less biological damage, deeper tissue penetration, and lower background fluorescence.[22,23] UCNP-based biosensors have demonstrated strong potential so far in medical diagnosis,[24,25] environmental monitoring,[26] and food safety.[27] UCNPs also provide a convenient visual window for flexible biosensors due to their visible fluorescence. Thus, a common camera or smartphone is required to read out the biosensor signal via image recognition with strong point-of-care (POC) prospects in the in situ detection. Although a few studies have reported the development of solid-phase biosensors based on UCNPs,[28,29] these biosensors still rely on expensive laboratory instruments. Hence, smartphone-based portable device and software might pave the path for the design of a flexible biosensor based on model strategy.

In this study, we constructed a regenerative flexible upconversion-luminescence biosensor for DES detection based on fluorescence resonance energy transfer (FRET) between dabcyl and UCNPs, and the signal of the biosensor realized dual readout based on a smartphone and a fluorescence spectrophotometer. As shown in Scheme 1, the UCNPs were synthesized by the high-temperature thermal decomposition method, and the flexible solid substrate was modified with the amino group by the piranha solution. To fabricate the biosensor, the cross-link glutaraldehyde method was used to assemble UCNPs and aptamer complementary DNA sequences (cDNA). Subsequently, using complementary base pairing, the dabcyl-labeled DES aptamer was bound to cDNA to form a FRET system via quenching the UL of UCNPs. When the target DES was coincubated with the flexible biosensor, the UL was gradually turned on. Due to the aptamer's preferential binding to DES, dabcyl was released from the biosensor's surface, thereby destroying the FRET system effectively. Accordingly, the biosensor's signal could be captured either as an image from a smartphone or spectrum from a fluorescence spectrophotometer. The dabcyl-labeled aptamer could be reassembled to regenerate the biosensor. Finally, a smartphone-based portable device equipped with an android application (APP) was developed for the designed biosensor.

2. MATERIALS AND METHODS

2.1. Reagents and Materials. $YCl_3{\cdot}6H_2O$, $YbCl_3{\cdot}6H_2O$, $TmCl_3{\cdot}6H_2O$ (99.99% pure), DES, dienestrol, hexestrol, bisphenol A, and 17β-estradiol were obtained from Aladdin Industrial Inc. (Shanghai, China). Methanol, oleic acid, 1-octadecene, sodium hydroxide, ammonium fluoride, sodium chloride, hydrochloric acid, sulfuric acid, ammonia, tetraethyl orthosilicate (TEOS), 3-aminopropyltriethoxysilane (APTES), glutaraldehyde aqueous solution (25%, v/v), phosphate buffer (PBS) solution (pH = 7.4), Tris-HCl buffer solution (pH = 8.5), and hydrogen peroxide were purchased from Sinopharm Chemical Reagent Co., Ltd. (Shanghai, China). Polydimethylsiloxane (PDMS, SYLGARD 184) was purchased from Dow Corning (Michigan, USA). The sequence and length of the DES aptamer selected in this research possessed the highest binding affinity to DES among the nine homologous families screened in the original study.[20] The dabcyl-labeled DES aptamer sequence (5′-GCC CTC TGA GGA TGC CGA AAA AGA AAA GAA ATT CTC TGG C-dabcyl-3′)[20] and DES

https://doi.org/10.1021/acs.analchem.1c03325
Anal. Chem. 2021, 93, 15667−15676

aptamer cDNA (5′−NH_2−AAA GCC AGA GAA TTT CTT TTC TTT TTC GGC ATC CTC AGA GGG C-3′) were synthesized by Sangon Biotech Co., Ltd. (Shanghai, China). The enzyme-linked immunosorbent assay (ELISA) kit was used as a standard control method for DES detection (CaoBenYuan Biotechnology Co., Ltd, Nanjing, China). Ultrapure water was obtained from a Milli-Q water purification system (Millipore, Billerica, MA, USA).

2.2. Instruments and Characterizations. The morphology and size of UCNPs and UCNPs@SiO_2 were characterized by JEM-2100 HR transmission electron microscopy (TEM, JEM-2100 JEOL, Japan). A D8 Advance X-ray diffractometer (BRUKER, Germany) was used to measure the X-ray diffraction (XRD) patterns of UCNPs at a 5°/min scanning rate in the 2θ range from 10 to 90°. The functionalized UCNPs@SiO_2 were characterized using the zeta potential recorded by a Malvern zetasizer Nano ZS90 (Malvern Instruments Ltd., U.K.) and Fourier transform infrared (FT-IR) spectrum collected by a Nicolet Nexus 470 FT-IR spectrophotometer (Thermo Electron Co., U.S.A.). The elemental distribution and morphology of the UCNPs@SiO_2-functionalized PDMS substrate was observed by field emission scanning electron microscopy (SEM, JSM-7800F, JEOL Ltd., Japan). Ultraviolet−visible (UV−vis) absorption spectrum was measured with a UV-2450 spectrophotometer (Shimadzu, Japan), and fluorescence lifetimes were measured with a phosphorescence lifetime spectrometer (FLS980, Edinburgh Instrument, U.K.) to validate the FRET between dabcyl and UCNPs. The upconversion fluorescence spectra were recorded by an RFS1000 fluorescence spectrophotometer with a 980 nm laser (Oceanhood opto-eletronics Co., Ltd., China). The images of the biosensor were photographed with a smartphone device (Mate 20, Huawei Technologies Co., Ltd., China) with an IR 750 shortwave pass filter (Beijing Yongxing Sensing Instrument., Ltd., Beijing, China). The absorbance of ELISA was determined by a microplate reader (Spark-20M, Tecan Trading AG, Switzerland).

2.3. Synthesis and Modification of $NaYF_4$:Yb^{3+},Tm^{3+} Nanoparticles. *2.3.1. Synthesis of UCNPs.* The $NaYF_4$:Yb^{3+},Tm^{3+} nanoparticles were synthesized according to a previously reported high-temperature thermal decomposition method with slight changes.[30] First, yttrium(III) chloride hexahydrate (0.795 mmol), ytterbium(III) chloride hexahydrate (0.2 mmol), and thulium(III) chloride hexahydrate (0.005 mmol) were ultrasonically dispersed in 10 mL of methanol. The mixture was transferred into a round-bottom flask (250.0 mL) that contained 15.0 mL of 1-octadecene and 6.0 mL of oleic acid. The solution was purged with nitrogen for 10.0 min and heated for 30.0 min at 160 °C with continuous stirring and allowed to cool subsequently under ambient conditions. Following that, sodium hydroxide (2.5 mmol) and ammonium fluoride (4 mmol) dispersed in methanol (10.0 mL) were added dropwise, and the mixed solution was heated to 75 °C for 40.0 min to fully volatilize the methanol solvent. After purged with nitrogen for 10 min, solution was heated for 10.0 min at 100 °C and later heated at 300 °C for 60.0 min with continuous stirring under nitrogen environment. Finally, the solution was cooled to room temperature and washed with a mixed solution of cyclohexane and ethanol (2:1, v/v) three times with simultaneous centrifugation at 8500 rpm for 10 min. The synthesized UCNPs were dried at 60 °C for further functionalization and characterization.

2.3.2. Modification of UCNPs. In order to functionalize UCNPs, the oleic acid-coated UCNPs synthesized by the thermal decomposition method ought to be changed into water-soluble UCNPs. First, ligand stripping of the oleic acid-coated UCNPs was performed based on reported methods.[31] The UCNPs (20.0 mg) were ultrasonically treated with 0.5 mL of hydrochloric acid solution (0.1 M) for 10.0 min. Next, the UCNPs were mixed with 60.0 mL of ethanol solution and ultrasonicated for 10.0 min. Subsequently, distilled water (10.0 mL) and aqueous ammonia (2.5 mL) were added and kept at 65 °C for 10.0 min to maintain the mixed solution in an alkaline environment. Then, 5.0 mL of ethanol containing 20.0 μL of TEOS was added, and the mixture was further allowed to react for 4.0 h at 65 °C. Finally, a mixture of 50.0 μL of APTES and 5.0 mL of ethanol was added into the flask and further heated for 2.0 h at 65 °C. A vigorous magnetic stirring was maintained throughout the reaction. The amino-modified water-soluble UCNPs were separated from the final solution by centrifugation at 8500 rpm for 5 min.

2.4. Development of the Flexible Biosensor. *2.4.1. Fabrication of UCNPs-Functionalized PDMS Substrate.* First, amino-functionalized PDMS substrate was obtained based on previous studies.[32] Briefly, the PDMS substrate (1 cm × 1 cm) was dipped in piranha solution (H_2O_2/H_2SO_4 = 1:3, v/v) at 40 °C for 1.0 min. The substrate was washed three times with distilled water and blown dry with nitrogen and then immersed in a mixture of APTES and ethanol (1:19, v/v) and heated at 70 °C for 3 h. The NH_2-modified PDMS substrate was obtained after rinsing with distilled water and drying with nitrogen. Subsequently, UCNPs were immobilized onto the PDMS substrate by the cross-link glutaraldehyde method.[33] UCNPs (10.0 mg) were ultrasonically dispersed in 5.0 mL of PBS buffer for 15 min, and then 1.25 mL of glutaraldehyde aqueous (25%, v/v) was added. The mixture was shaken rapidly in the dark for 2.0 h to activate the amino groups on the UCNP surface. Afterward, the UCNPs were collected by centrifugation followed by washing and redispersion in PBS buffer. To fabricate the UCNPs-functionalized PDMS substrate (UCNPs−PDMS), each PDMS substrate was coincubated with 2.0 mL of UCNP (0.8 mg/mL) dispersion for 12 h and then rinsed three times with PBS buffer and dried with nitrogen.

2.4.2. Preparation of Biomolecular-Functionalized UCNPs−PDMS. The DES aptamer cDNA modified with the amino group was also immobilized onto UCNPs−PDMS using the cross-link glutaraldehyde method. UCNPs−PDMS were activated in the same way as UCNPs. The cleaned activated UCNPs−PDMS substrate was reimmersed in 2.0 mL of PBS buffer, a fraction of 30 μL of DES aptamer cDNA was introduced into it, and the mixture was kept at 37 °C for 12 h under slow stirring. The cDNA-functionalized UCNPs−PDMS substrate was reimmersed in 2.0 mL of PBS buffer. Following triple rinse, 30 μL of the dabcyl-labeled DES aptamer was added and allowed to heat for 95 °C for 3.0 min in a water bath. The solution was gently shaken and gradually cooled below 65 °C while maintaining an agitation at 37 °C. The whole process of binding the DES aptamer to cDNA took 1.0 h based on complementary base pairing. Finally, the flexible biosensor was obtained by rinsing with PBS buffer three times and drying with nitrogen.

2.5. Detection of DES by the Flexible Biosensor. The prefabricated aptamer-cDNA-UCNPs-PDMS sensors were immersed in 2.0 mL of Tris-HCl buffer (pH 8.5). Under

https://doi.org/10.1021/acs.analchem.1c03325
Anal. Chem. 2021, 93, 15667−15676

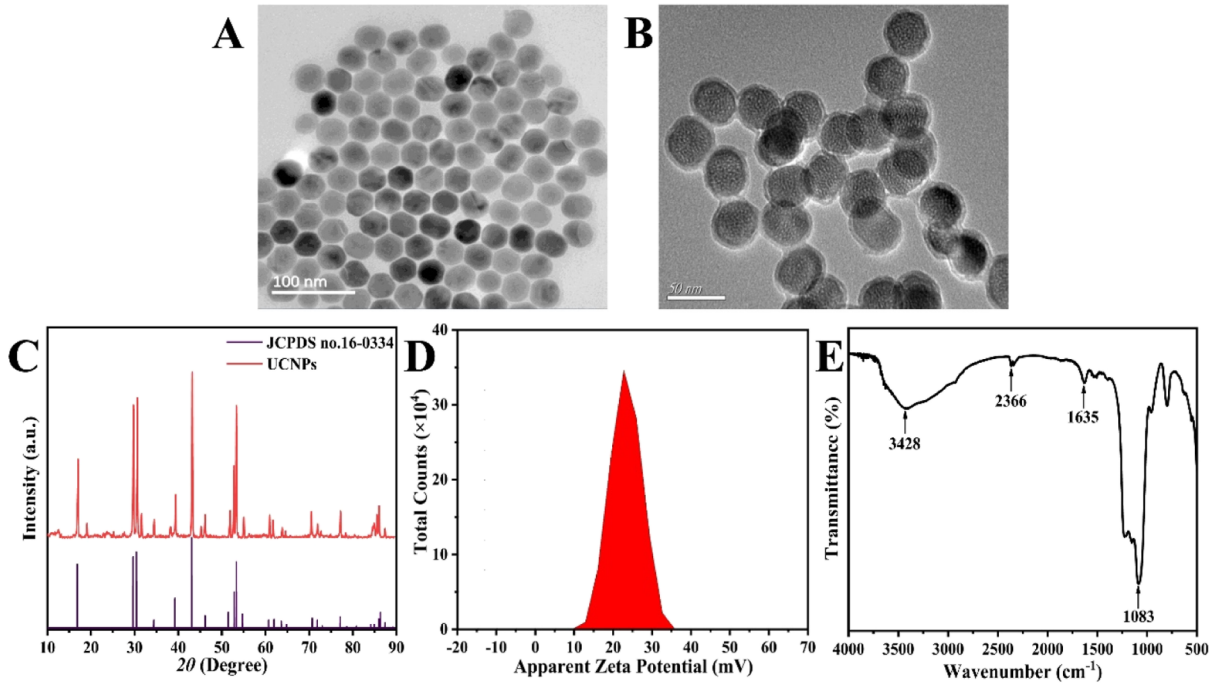

Figure 1. Characterization of UCNPs: (A) TEM image of UCNPs; (B) TEM image of UCNPs@SiO_2; (C) XRD pattern of UCNPs; (D) zeta potential of UCNPs-NH_2; (E) FT-IR spectra of UCNPs-NH_2.

optimal conditions, various concentrations of DES standard solution (0.05−500 ng/mL) were added and incubated with the biosensor at 37 °C for 25 min. Following triple rinse to ensure adequate removal of the aptamer and DES conjugate, the biosensors were dried with nitrogen for 1.0 min. Finally, the biosensor response was monitored using a spectrofluorometer and a smartphone device, respectively. As shown in Figure S1, a simple platform for image acquisition of the biosensor was designed. The smartphone captured the images from above the biosensor, while the 980 nm excitation light radiated beneath it (Figure S1A). An IR 750 shortwave pass filter (near-infrared filter) was attached onto the smartphone camera to prevent the excitation light from influencing image acquisition, as demonstrated in Figure S1B. This ensures light with a wavelength greater than 750 nm from passing through. The parameters of image acquisition are shown in Figure S1C. In addition, performance of the near-infrared filter was also evaluated as illustrated in Figure S2.

2.6. Specificity, Anti-Interfering, and Regeneration of the Biosensor. To explore the specificity of the developed flexible biosensor, several relevant structural analogues and common estrogens (dienestrol, hexestrol, bisphenol A, and 17β-estradiol) were investigated in relatively large excess by the developed biosensor. These estrogens (50 ng/mL) were tested simultaneously with DES (5 ng/mL) to verify the anti-interference capability of the biosensor. The used biosensors were also regenerated by incubation with dabcyl-labeled DES aptamers. Thus, the same biosensor was cyclically tested for DES (5 ng/mL) and regenerated to evaluate its regeneration ability.

2.7. Analysis of DES in Spiked Samples. Prawn, fish, and river water were selected to detect the DES residue levels in the real sample matrices for demonstrating the viability of this developed biosensor. The prawn and fish were purchased from Auchan supermarket (Zhenjiang City, Jiangsu Province, China), and the river water samples were obtained from the Zhenjiang YuDai river. The samples were spiked with three concentration levels (1, 5, and 10 ng/mL) of DES standard solution and pretreated for quantitative determination using the proposed method. The prawn and fish samples were pretreated in accordance with the ELISA kit instructions. In brief, a total of 2 g of samples was homogenized by a homogenizer followed by the addition of 6 mL of a mixture of acetonitrile and acetone (4:1, v/v). The mixture was shaken for 2 min and then centrifuged at 4000 rpm for 10 min. Next, 3 mL of supernatant was taken and dried with nitrogen at 60 °C, which was redissolved in 0.5 mL of chloroform. Then, 2 mL of sodium hydroxide solution (2 M) was added to the test solution, shaken for 30 s, and centrifuged at 4000 rpm for 5 min. Afterward, 1 mL of supernatant was taken, and 200 μL of phosphoric acid (6 M) was added to it followed by gentle shaking for 5 s. The mixture was extracted with 3 mL of acetonitrile followed by shaking for 2 min and centrifugation at 4000 rpm for 10 min under ambient conditions. 1.5 mL of the upper organic phase was collected after centrifugation and dried with nitrogen at 60 °C. Finally, the residue was redissolved in 1 mL of methanol solution (40%, v/v) and vibrated for 2 min, and 50 μL of solution was taken for testing. Dilution factor of the pretreated samples is4. The river water was centrifuged at 10,000 rpm for 5 min and filtered before detection to remove impurities and diluted four times as well. The ELISA methods are detailed in the Supporting Information

2.8. Statistical Analysis. The data from the biosensor were triple duplicated and calculated as mean ± standard deviation (SD). Upconversion fluorescence spectral data were analyzed on OriginPro 2018C (OriginLab, Northampton, MA, U.S.A). The region of interest (ROI) interception and information extraction of the biosensor images were implemented by MATLAB (Version R2014b, Mathworks, Natick, MA, USA). As illustrated in Figure S3, the 200 × 200-pixel ROI was intercepted from the original image for

https://doi.org/10.1021/acs.analchem.1c03325
Anal. Chem. 2021, 93, 15667−15676

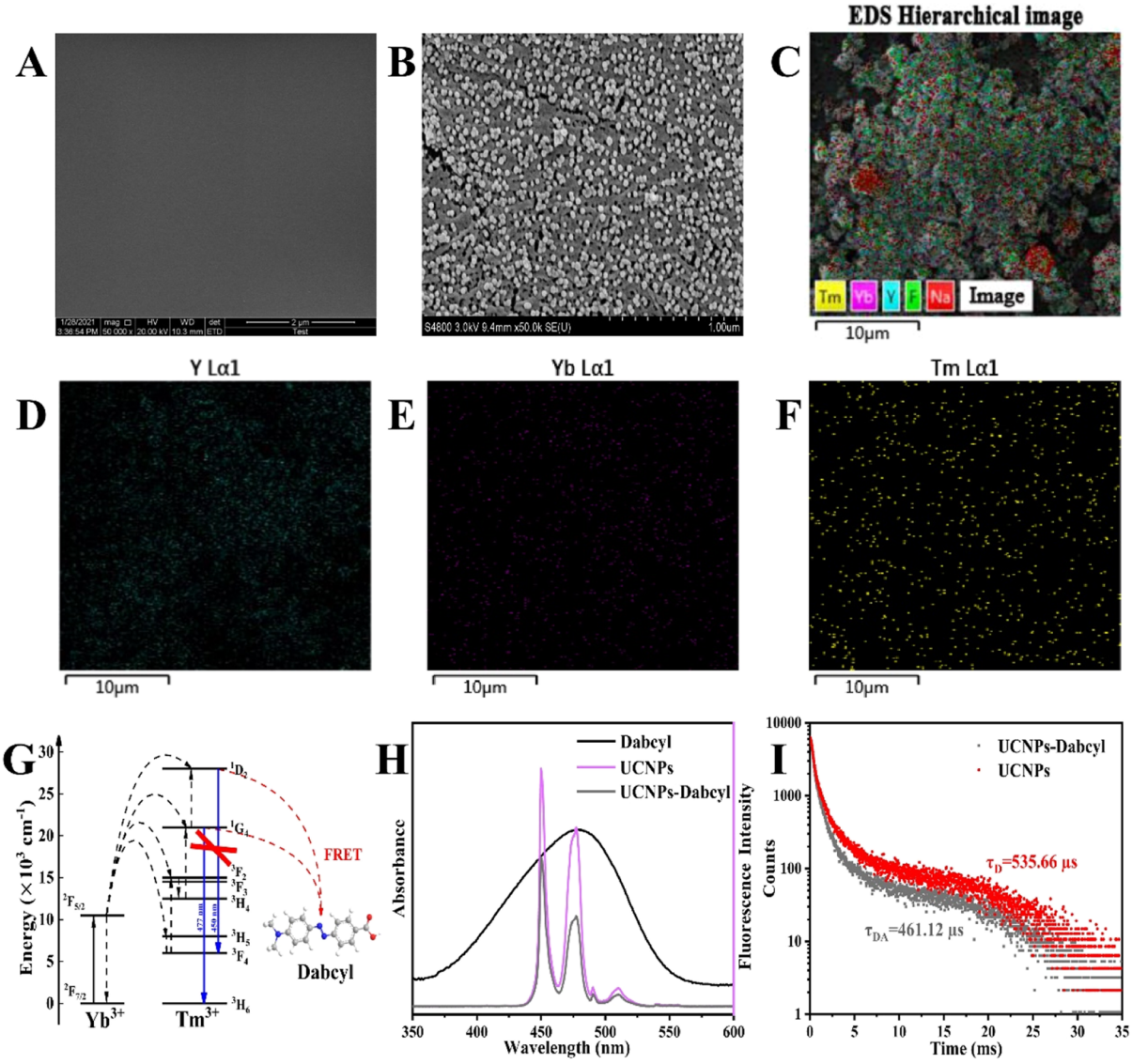

Figure 2. Characterization of the PDMS substrate and validation of the FRET system: (A) SEM image of the PDMS substrate; (B) SEM image of UCNPs-functionalized PDMS substrate; (C) EDS hierarchical image of UCNPs-functionalized PDMS substrate; (D–F) elemental mapping images of Y, Yb, and Tm; (G) excitation and FRET mechanism between UCNPs and dabcyl; (H) comparison of fluorescence spectra of UCNPs and UV–vis absorption spectra of dabcyl; (I) fluorescence lifetime curve of UCNPs and UCNPs–dabcyl.

extracting effective information. Two-tailed *t*-test between the results of spiked-in samples by the proposed method and ELISA was performed to test their significance.

3. RESULTS AND DISCUSSION

3.1. Synthesis and Characterization of the Biosensor.

TEM, XRD, zeta potential, and FT-IR were used to characterize the morphology, size, crystal structure, and surface functional groups of UCNPs. As demonstrated in Figure 1, the TEM image (Figure 1A) revealed that the oleic acid-coated UCNPs prepared by the high-temperature thermal decomposition method possessed a good degree of dispersion in cyclohexane with a hexagonal nanoparticle structure of diameter of 31.7 ± 0.9 nm (n = 6). Further, as demonstrated in (Figure 1C), the XRD pattern confirmed that the diffraction peaks of UCNPs were highly consistent with those of β-$NaYF_4$ crystal (JCPDS standard card no.16-0334), indicating high crystallinity of the prepared hexagonal UCNPs. The modified water-soluble UCNPs had a particle size of 38.7 ± 1.3 nm and a silica shell thickness of 3.1 ± 0.5 nm (n = 6) (Figure 1B), where the uniform silica-coated shell provided good water solubility for broader practical applications. The zeta potential of UCNPs showed that the nanoparticles dispersed in distilled water has a positive charge of 23.2 ± 3.97 mV (Figure 1D), indicating that the nanoparticles were stable due to amination of its surface. Further, FT-IR spectroscopy was used to characterize the functional groups on the surface of silica-coated UCNPs. As shown in Figure 1E, the transmission bands centered at 3428 and 1635 cm^{-1} were ascribed to the stretching and bending vibration bands of N–H, respectively. The high-intensity peaks at 1083 and 2366 cm^{-1} corresponded to the stretching vibration bands of Si–O–Si and Si–H.[34] These characteristic peaks indicated that UCNPs were successfully coated with silica and modified with amino groups, imparting high water solubility to the nanoparticles.

SEM images, EDS, elemental mapping, UV–vis spectra, fluorescence spectrum, and fluorescence lifetime test were used to further characterize the morphology of UCNPs-function-

https://doi.org/10.1021/acs.analchem.1c03325
Anal. Chem. 2021, 93, 15667–15676

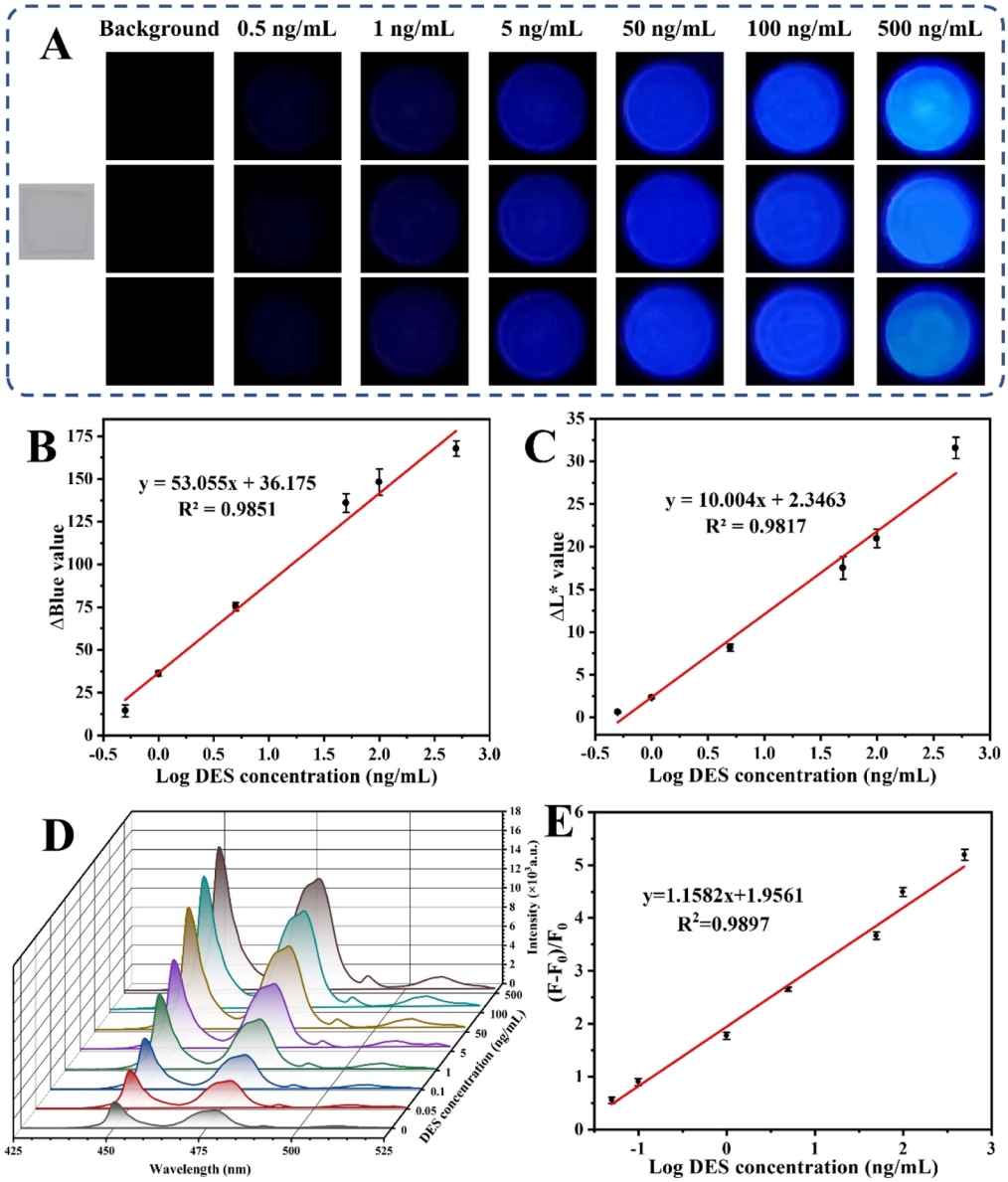

Figure 3. Calibration curves of DES detection: (A) Images of the flexible biosensor in the presence of different concentrations of DES; (B,C) plots of blue value and *L** value of images with the various concentrations of DES (0.5, 1, 5, 50, 100, and 500 ng/mL); (D) upconversion fluorescence spectra of the flexible biosensor in the presence of different concentrations of DES; (E) plot of fluorescence recovery efficiency with various concentrations of DES (0.05, 0.1, 1, 5, 50, 100, and 500 ng/mL).

alized PDMS substrate and verify the FRET system. As illustrated in Figure 2, the SEM image (Figure 2A) revealed that the bare PDMS substrate was smooth and flat. Afterward, UCNPs were uniformly loaded on the surface of the PDMS substrate, as shown in Figure 2B. Furthermore, EDS and elemental mapping were used to confirm the composition and distribution of elements on the surface of the UCNPs−PDMS substrate. The EDS hierarchical image (Figure 2C) of elements in $NaYF_4$:Yb^{3+},Tm^{3+} nanoparticles and energy-dispersive X-ray elemental mapping images of Y, Yb, and Tm (Figure 2D−F) revealed a reasonable composition and uniform distribution of elements. These data indicate that the UCNPs-functionalized PDMS substrate have a satisfactory performance as the fluorescence reporting signal. The changes in the fluorescence signal were caused by the FRET effect between the UCNPs and dabcyl (Figure 2G). As shown in Figure 2H, the characteristic emission peaks at 450 and 477 nm were assigned to the $^1D_2 \rightarrow {}^3H_6$ and $^1G_4 \rightarrow {}^3H_6$ transitions of Tm^{3+} ions, respectively.[35] The UV−vis spectrum of dabcyl revealed a maximum absorption peak at 480 nm (Figure 2H), and an overlap between the absorption peak of dabcyl and the emission peak of UCNPs confirms the formation of the FRET system. As presented in Figure 2I, the fluorescence lifetimes of UCNPs in the absence and presence of the acceptor dabcyl were measured to be τ_D = 535.66 μs and τ_{DA} = 461.12 μs, respectively.

3.2. Design Scheme of the DES Biosensor. As illustrated in Scheme 1, the basic procedure of the proposed flexible biosensor consists of three stages as follows: (I) fabrication of the flexible biosensor (aptamer-cDNA−UCNPs−PDMS); (II) detection of target DES by the proposed biosensor; and (III) regeneration of the biosensor. Based on the spectral overlap and spatial proximity caused by complementary base pairing, UCNPs and dabcyl served as the

https://doi.org/10.1021/acs.analchem.1c03325
Anal. Chem. 2021, 93, 15667−15676

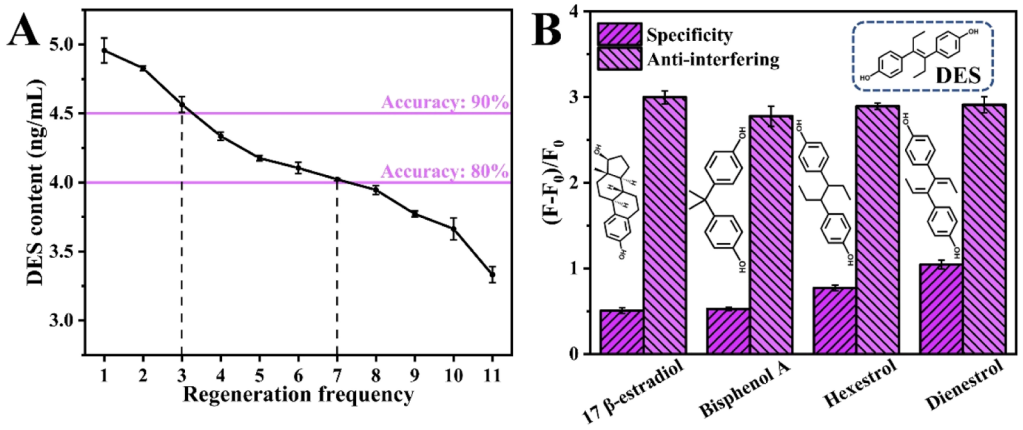

Figure 4. Performance evaluation of the flexible biosensor: (A) Regeneration of the flexible biosensor for DES detection; (B) specificity and anti-interfering of the designed flexible biosensor. The concentrations of DES and other interferents are 5 and 50 ng/mL, respectively.

donor and acceptor pairs to constitute FRET system, resulting in efficient quenching of UL. This FRET was annihilated when the biosensor was incubated with the test solution due to the stronger affinity of the aptamer for DES, which caused the UL turn-on at 477 nm. The recovered fluorescence was proportional to the content of target DES. Therefore, the recovery of fluorescence intensity of the biosensor at 477 nm was monitored by a spectrofluorometer to reflect the DES concentration. On the other hand, the images of the biosensor were read in the RGB mode (R represents red value, G represents green value, and B represents blue value) and $L^*a^*b^*$ mode (L^* represents lightness, a* indicates redness and greenness, and b* indicates yellowness and blueness),[36] where B and L^* values were proportional to the fluorescence intensity and were positively correlated with the concentration of target DES.

The overlap between the dabcyl absorption peak the UCNP emission peak at 477 nm resulted in the UL quenching of UCNPs via FRET (Figure 2G). The fluorescence quenching of UCNPs−dabcyl was attributed to FRET from Tm^{3+} to dabcyl via dabcyl-labeled DES aptamer combined with cDNA assembled on the surface of UCNPs, as shown in Figure 2H. Furthermore, the luminescence decay curves and lifetimes of UCNPs were determined in the presence and absence of the acceptor dabcyl (Figure 2I). The FRET efficiency (E) is related to the fluorescence lifetime of the UCNPs as eq 1[37]

$$E = 1 - \frac{\tau_{DA}}{\tau_D} \quad (1)$$

where τ_{DA} and τ_D are the donor (UCNPs) fluorescence lifetimes in the presence and absence of the acceptor (dabcyl), respectively. The FRET efficiency was calculated to be 13.9% according to eq 1. Therefore, the data confirmed the design of the biosensor to be based on the FRET process.

3.3. Optimization of the Biosensor and Detection Conditions. The loading quantity of UCNPs and dabcyl on the PDMS substrate was optimized in order to prepare a high-performance biosensor with improved sensitivity. The results of the parameters optimized in this work can be seen in Figure S4. The concentration of the UCNPs and their influence on the UL intensity changes of PDMS substrates after incubation with 2 mL were investigated in the range 0.1−0.9 mg/mL (Figure S4A). The fluorescence intensity of PDMS substrates gradually increased with the increase in the concentration of the UCNPs till 0.8 mg/mL and remained stable afterward. Thus, an optimal 0.8 mg/mL concentration of UCNPs was used to modify onto the PDMS substrate for subsequent experiments. Further, the influence of the dabcyl-labeled aptamer volume (5.0−35.0 μL) on the UL intensity of the biosensor was investigated. As exhibited in Figure S4B, the degree of fluorescence quenching of the biosensor as a function of the dabcyl-labeled aptamer concentration shows a gradual decrease until being stable at 25 μL and onward. Therefore, 30 μL of dabcyl-labeled aptamer was incubated with cDNA−UCNPs−PDMS for subsequent experiments to ensure an enhanced optimal quenching effect. Furthermore, the pH value, ionic strength, and incubation time were also optimized. As illustrated in Figure S4C, the influence of Tris-HCl buffer in the range 7.0−10.0 revealed a gradual increase in the UL turn-on intensity till pH 8.5 and declined afterward at a fixed concentration of DES (5 ng/mL). The binding efficiency was also investigated for possible ionic strength via adding different concentrations of sodium chloride. The results revealed that the highest UL turn-on intensity was observed at 0.05 M (Figure S4D). Finally, the incubation time (1.0−30 min) was also optimized at a fixed DES concentration (5 ng/mL). The results in Figure S4E demonstrated that the UL intensity increased gradually over time, the aptamer hybridization with DES was completed in 25.0 min, and the conjugates were separated from the biosensor. Hence, the subsequent experiments were performed on the optimized pH 8.5 Tris−HCl buffer, ionic strength 0.05 M sodium chloride, and 25.0 min incubation time.

3.4. Detection of DES Based on the Flexible Biosensor. Analytical figure of merits of the developed flexible biosensor for DES determination were investigated under the optimized experimental conditions. The ROI of fluorescence images of biosensor incubated with various concentrations of DES standard solution were obtained under the optimal experimental conditions as shown in Figure 3A. As can be seen in the images, the brightness increased gradually as the concentration of DES increased. It was found that the blue and L^* values in the images were strongly correlated with the logarithmic concentration of the target DES. This correlation between DES concentration against the blue values and L^* values of the biosensor images are plotted in Figure 3B,C, respectively. The calibration curve can be calculated as ΔB (deducting blank background) = 53.055x + 36.175 with R^2 = 0.9851 and ΔL^* (deducting blank background) = 10.004x + 2.3463 with R^2 = 0.9817. The

https://doi.org/10.1021/acs.analchem.1c03325
Anal. Chem. 2021, 93, 15667−15676

Table 1. Determination of DES in Real Environment and Foodstuff Samples[a,b,c,d]

		this work						ELISA				
		imaging			fluorescence							
sample	spiked levels (ng/mL)	found ± SD (ng/mL)	recovery (%)	CVs (%)	found ± SD (ng/mL)	recovery (%)	CVs (%)	found ± SD (ng/mL)	recovery (%)	CVs (%)	P_1	P_2
river water	1				0.96 ± 0.08	95.81	8.65	0.86 ± 0.07	86.30	7.62	0.94	0.89
	5	4.53 ± 0.58	90.70	12.82	4.90 ± 0.38	97.95	7.69	4.86 ± 0.27	97.23	5.48		
	10	9.50 ± 0.32	94.96	3.42	9.12 ± 0.50	91.16	5.54	9.23 ± 0.38	92.33	4.15		
prawn	1				0.79 ± 0.07	79.17	8.60	0.83 ± 0.04	83.01	5.15	0.46	0.71
	5	4.18 ± 0.08	83.55	1.95	4.26 ± 0.25	85.12	5.90	4.35 ± 0.11	86.89	2.60		
	10	8.57 ± 0.41	85.72	4.77	8.65 ± 0.43	86.5	4.98	8.58 ± 0.37	85.77	4.37		
fish	1				0.86 ± 0.05	85.64	5.45	0.73 ± 0.004	72.84	0.48	0.63	0.89
	5	4.06 ± 0.10	81.15	2.35	4.22 ± 0.28	84.47	6.63	3.87 ± 0.06	77.48	1.15		
	10	7.79 ± 0.34	77.91	4.32	8.10 ± 0.33	80.96	4.11	8.71 ± 0.26	87.07	3.04		

[a]SD: standard deviation; CVs: coefficients of variation. [b]P_1: two-tailed *t*-test result between imaging and ELISA method. [c]P_2: two-tailed *t*-test result between fluorescence and ELISA method. [d]$P > 0.05$: there were no significant difference.

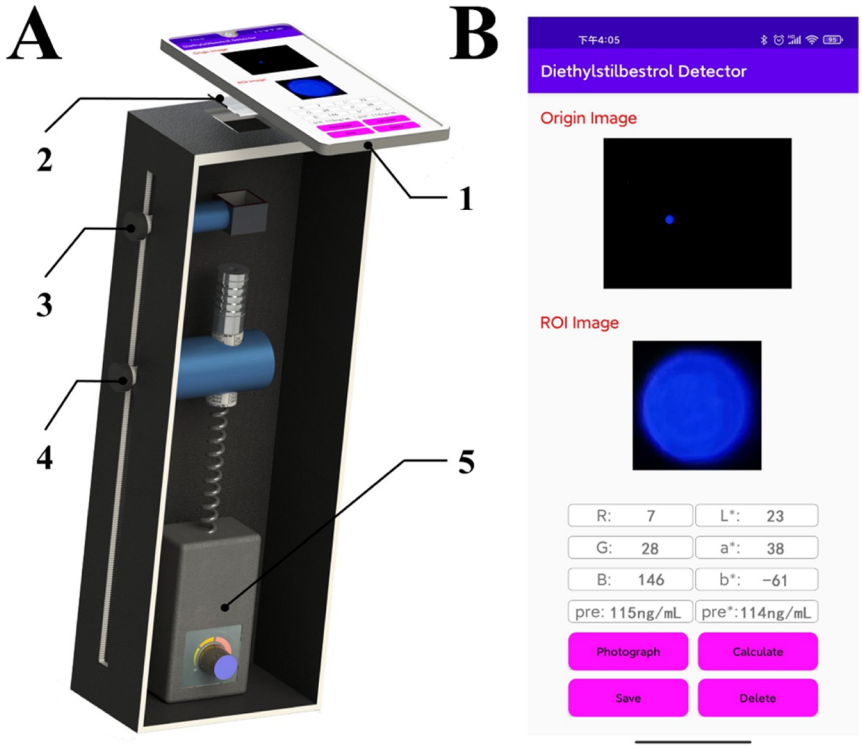

Figure 5. Portable device and software: (A) Portable equipment consists of (1) a smartphone, (2) an IR 750 shortwave pass filter (infrared filter), (3) a flexible biosensor support platform, (4) a knob for adjusting the focal length of the laser, and (5) a portable 980 nm laser; (B) interface of smartphone application based on Android platform.

calculated limit of detection (LOD) of the biosensor for the blue value was 0.063 ng/mL and for the L^* value was 0.024 ng/mL based on $3\delta/S$ (where δ is the standard deviation of n (n = 10) control measurements and S is the slope of the calibration curve). To validate the smartphone imaging method's accuracy, the fluorescent signal from the flexible biosensor was also collected for comparison. The upconversion fluorescence spectra at 477 nm for varying concentrations (0.05−500 ng/mL) of DES standard solution are demonstrated in Figure 3D. The calibration plot of the increased UL intensity at 477 nm against the concentrations of DES is shown in Figure 3E. The changes in UL intensity are expressed as the recovery efficiency $[(F-F_0)/F_0$, where F and F_0 represent the UL intensity at 477 nm in the presence and absence of DES, respectively]. A good linear relationship between the recovery efficiency of UL intensity and the logarithm concentration of DES was observed (0.05−500 ng/mL), with a regression equation as $y = 1.1582x + 1.9561$, and correlation coefficient (R^2) = 0.9897. In addition, the LOD was calculated to be 0.032 ng/mL by $3\delta/S$. It can be concluded that the smartphone imaging results were comparable in accuracy with the designed biosensor strategy. Thus, the designed flexible biosensor demonstrated good performance for the quantitative detection of target DES, and the signal readout for the designed strategy could be implemented on a smartphone and a fluorescence spectrophotometer.

3.5. Regeneration, Specificity, and Anti-Interfering of the DES Biosensor. To investigate the regenerative ability of

https://doi.org/10.1021/acs.analchem.1c03325
Anal. Chem. 2021, 93, 15667−15676

the designed biosensors, it was cyclically tested at 5.0 ng/mL DES concentration and reincubated with Dabcyl-labeled aptamers. The results are shown in Figure 4A; the detective accuracy decreased gradually with the increase of regeneration times, which may be caused by the shedding of UCNPs on the surface of the PDMS substrate or the cracking of the DES aptamer cDNA. Nevertheless, the designed biosensor can be regenerated seven times with a threshold of 80% accuracy. Additionally, several structural analogues and common estrogens (dienestrol, hexestrol, bisphenol A, and 17β-estradiol) were introduced in the recommended procedure for DES detection to verify the specificity and selectivity of the developed biosensor. As shown in Figure 4B, all these estrogens caused negligible influence on the fluorescence signal despite its presence in excess concentration. The restored fluorescence at 5 ng/mL DES concentration in the presence of other structural analogues and estrogens was therefore influenced to a negligible extent. In addition, seven different batches of the UCNPsthe -modified PDMS substrate were prepared to verify the repeatability of the biosensor. As demonstrated in Figure S5, the upconversion fluorescence intensities of substrates prepared by different batches were almost consistent, with a relative SD of 3.26%. The results showed that the UCNPs-modified PDMS substrate possessed acceptable reproducibility. Thus, it can be concluded that the designed flexible biosensor for DES determination can be extended to complex matrices.

3.6. DES Determination in Real Samples. The applicability of the proposed flexible biosensor was investigated in real river water, prawn, and fish samples for various spiked DES concentrations (1.0−10.0 ng/mL). The real samples were spiked with different DES concentrations and were subjected to analysis by the proposed recommended procedure and further validated by the standard ELISA method. The calibration curve for DES detected by ELISA was fitted as Figure S6. The detection values were calculated through collecting the corresponding signals (fluorescence intensity, blue value, L^* value, and absorbance) and then substituting them for the linear formulas. As listed in Table 1, the real samples with three levels concentrations of DES were detected with recoveries in the range of 79.17−97.95% and coefficient of variations (CVs) in the range of 4.11−8.65% based on the fluorescence method. Simultaneously, the recoveries ranged from 77.91 to 94.96% and CVs ranged from 1.95 to 12.84% based on smartphone imaging data. The statistical treatment via students' t-test revealed no significant difference between tested results of the proposed flexible biosensor based on the spectrofluorometer, smartphone imaging, and ELISA method at $p > 0.05$ (Table 1), and the correlations of these methods were plotted as Figure S7. Hence, the results demonstrated the applicability of the dual methods for the DES detection in real environment and foodstuff samples.

3.7. Device Design and Software Development. In order to realize POC testing of the constructed flexible biosensor, we designed a supporting portable and economical equipment and software, as illustrated in Figure 5. The device consists of a portable 980 nm laser, a smartphone, a near-infrared filter, and a self-made platform (Figure 5A). The power and focal length of the laser can be adjusted freely to ensure the best excitation effect of the constructed flexible biosensor. Furthermore, a mobile application based on the Android platform was developed, as exhibited in Figure 5B. The software collects the images of the constructed flexible biosensor, automatically cuts the ROI, and extracts the image information (color and brightness), which is substituted into the linear formulas to display the results of DES detection. The image processing algorithm and core code of the software are presented in the Supporting Information. For comparative purposes, Table S1 summarizes the advantages and disadvantages of several reported sensors for DES detection. The LOD of the proposed flexible biosensor was lower than those of most of the previously reported sensors but significantly higher than that of the electrochemical immunosensor. However, the developed flexible biosensor has the advantages of facile operation, regeneration, and portability with an APP based on smartphone. The proposed platform might be helpful for POC testing and in situ detection.

4. CONCLUSIONS

In this work, a regenerative flexible upconversion-fluorescence biosensor was designed for the detection of DES residue in the environment and food samples. The proposed biosensor can realize dual-mode signal readout based on images from a smartphone and spectra from a fluorescence spectrometer. Good linear relationships were achieved based on the images ($\Delta B = 53.055x + 36.175$, $R^2 = 0.9851$; $\Delta L^* = 10.004x + 2.3463$, $R^2 = 0.9817$) and spectra ($y = 1.1582x + 1.9561$, $R^2 = 0.9897$), respectively. The designed biosensor offered high sensitivity with an LOD of 0.024 ng/mL and selectivity in the presence of most structural analogues of DES. The dual-mode method was applied in real environmental and food samples with the recovery range of 77.91−97.95%. The proposed strategies were validated by standard ELISA method in terms of statistical t-test with no significant difference. In comparison to solution-phase biosensors, the designed flexible biosensor can be regenerated seven times with a threshold accuracy of 80% and has additional advantages of stability, portability, and cost-effectiveness. Furthermore, POC and on-site detection of DES are expected to be easily implemented on the developed portable device and android APP. However, there may be more than one type of EDC present in environment and foodstuff. Hence, the development of flexible biosensors for simultaneous detection of multiple EDC types will further expand its practicability.

■ ASSOCIATED CONTENT

Supporting Information

The Supporting Information is available free of charge at https://pubs.acs.org/doi/10.1021/acs.analchem.1c03325.

Detection steps of DES by the ELISA method; simple image acquisition platform; performance test of the near-infrared filter; ROI cropping of the flexible biosensor images; optimization of the biosensor and detection parameters; reproducibility of the preparation of the UCNPs-modified PDMS substrate; calibration curve of DES determined by the ELISA method; correlation analysis between fluorescence, imaging, and the ELISA method; comparison of this work with other reported detection methods; and core code of software based on Android platform (PDF)

■ AUTHOR INFORMATION

Corresponding Authors

Qin Ouyang − *School of Food and Biological Engineering, Jiangsu University, Zhenjiang 212013, P. R. China;*

https://doi.org/10.1021/acs.analchem.1c03325
Anal. Chem. 2021, 93, 15667−15676

orcid.org/0000-0002-8469-3099; Phone: +86-511-88790318; Email: oyqyf@ujs.edu.cn; Fax: +86-511-88780201

Quansheng Chen − *School of Food and Biological Engineering, Jiangsu University, Zhenjiang 212013, P. R. China;* orcid.org/0000-0003-2498-3278; Email: qschen@ujs.edu.cn

Authors

Jizhong Wu − *School of Food and Biological Engineering, Jiangsu University, Zhenjiang 212013, P. R. China*

Waqas Ahmad − *School of Food and Biological Engineering, Jiangsu University, Zhenjiang 212013, P. R. China*

Jingui Zhang − *School of Food and Biological Engineering, Jiangsu University, Zhenjiang 212013, P. R. China*

Mingming Zhang − *School of Food and Biological Engineering, Jiangsu University, Zhenjiang 212013, P. R. China*

Complete contact information is available at: https://pubs.acs.org/10.1021/acs.analchem.1c03325

Author Contributions

J.W. handled conceptualization, methodology, investigation, validation, visualization, formal analysis, writing-original draft, and writing-review and editing. W.A. handled formal analysis and writing-review and editing. Q.O. handled data curation, funding acquisition, writing-review and editing, and project administration. J.Z. handled methodology and investigation. M.Z. handled investigation. Q.C. handled resources, funding acquisition, supervision, and project administration.

Notes

The authors declare no competing financial interest.

■ ACKNOWLEDGMENTS

This work was financially supported by the Natural Science Foundation of Jiangsu Province (BK20190100), the Self-innovation Fund Project of Agricultural Science and Technology in Jiangsu Province (CX(20)2005), the Key R&D Program of Jiangsu Province (BE2020379), and the Project of Faculty of Agricultural Equipment of Jiangsu University.

■ REFERENCES

(1) Diamanti-Kandarakis, E.; Bourguignon, J.-P.; Giudice, L. C.; Hauser, R.; Prins, G. S.; Soto, A. M.; Zoeller, R. T.; Gore, A. C. *Endocr. Rev.* **2009**, *30*, 293−342.

(2) Reed, C. E.; Fenton, S. E. *Birth Defects Res., Part C* **2013**, *99*, 134−146.

(3) Xu, Z.; Sun, T.; He, H.; Liu, W.; Fan, L.; Zhao, L.; Wu, X.; Han, Z.; Zhang, Y.; Wang, Q.; Ning, B.; Gao, Z. *Food Nutr. Sci.* **2021**, *9*, 1824−1830.

(4) Wang, L.-H.; Chen, L.-R.; Chen, K.-H. *Int. J. Mol. Sci.* **2021**, *22*, 4013.

(5) Johansson, H. K. L.; Christiansen, S.; Draskau, M. K.; Svingen, T.; Boberg, J. *Reprod. Toxicol.* **2021**, *101*, 9−17.

(6) Hunter, D.; Heng, K.; Mann, N.; Anand-Ivell, R.; Ivell, R. *Int. J. Mol. Sci.* **2021**, *22*, 4163.

(7) Hoover, R. N.; Hyer, M.; Pfeiffer, R. M.; Adam, E.; Bond, B.; Cheville, A. L.; Colton, T.; Hartge, P.; Hatch, E. E.; Herbst, A. L.; Karlan, B. Y.; Kaufman, R.; Noller, K. L.; Palmer, J. R.; Robboy, S. J.; Saal, R. C.; Strohsnitter, W.; Titus-Ernstoff, L.; Troisi, R. *N. Engl. J. Med.* **2011**, *365*, 1304−1314.

(8) Zhang, J.; Zang, L.; Wang, T.; Wang, X.; Jia, M.; Zhang, D.; Zhang, H. *Food Chem.* **2020**, *333*, 127529.

(9) Zhao, W.-R.; Xu, Y.-H.; Kang, T.-F.; Zhang, X.; Liu, H.; Ming, A.-J.; Cheng, S.-Y.; Wei, F. *Biosens. Bioelectron.* **2020**, *155*, 112102.

(10) Wang, X.; Ding, H.; Yu, X.; Shi, X.; Sun, A.; Li, D.; Zhao, J. *Talanta* **2019**, *197*, 98−104.

(11) Wu, T.; Yan, T.; Zhang, X.; Feng, Y.; Wei, D.; Sun, M.; Du, B.; Wei, Q. *Biosens. Bioelectron.* **2018**, *117*, 575−582.

(12) Guan, W.; Zhou, W.; Lu, J.; Lu, C. *Chem. Soc. Rev.* **2015**, *44*, 6981−7009.

(13) Su, Y.; Yang, T.; Zhao, X.; Cai, Z.; Chen, G.; Yao, M.; Chen, K.; Bick, M.; Wang, J.; Li, S.; Xie, G.; Tai, H.; Du, X.; Jiang, Y.; Chen, J. *Nano Energy* **2020**, *74*, 104941.

(14) Xue, J.; Noh, H. M.; Choi, B. C.; Park, S. H.; Kim, J. H.; Jeong, J. H.; Du, P. *Chem. Eng. J.* **2020**, *382*, 122861.

(15) Trigo-López, M.; Muñoz, A.; Mendía, A.; Ibeas, S.; Serna, F.; García, F. C.; García, J. M. *Sens. Actuators, B* **2018**, *255*, 2750−2755.

(16) Zhu, A.; Ali, S.; Xu, Y.; Ouyang, Q.; Chen, Q. *Biosens. Bioelectron.* **2021**, *172*, 112806.

(17) Li, H.; Chen, Q.; Mehedi Hassan, M.; Chen, X.; Ouyang, Q.; Guo, Z.; Zhao, J. *Biosens. Bioelectron.* **2017**, *92*, 192−199.

(18) Jiang, Q.; Zhang, D.; Cao, Y.; Gan, N. *J. Electroanal. Chem.* **2017**, *789*, 1−8.

(19) Li, J.; Shan, X.; Jiang, D.; Chen, Z. *Analyst* **2020**, *145*, 3306−3312.

(20) Wang, M.; Wang, Q.; Li, X.; Lu, L.; Du, S.; Zhang, H. *Microchem. J.* **2020**, *159*, 105354.

(21) Wang, P.; Wang, A.; Hassan, M. M.; Ouyang, Q.; Li, H.; Chen, Q. *Sens. Actuators, B* **2020**, *320*, 128434.

(22) Hu, W.; Chen, Q.; Li, H.; Ouyang, Q.; Zhao, J. *Biosens. Bioelectron.* **2016**, *80*, 398−404.

(23) Rong, Y.; Ali, S.; Ouyang, Q.; Wang, L.; Wang, B.; Chen, Q. *Food Chem.* **2021**, *351*, 129215.

(24) Zhang, X.-W.; Liu, M.-X.; He, M.-Q.; Chen, S.; Yu, Y.-L.; Wang, J.-H. *Anal. Chem.* **2021**, *93*, 6437−6445.

(25) Guo, J.; Chen, S.; Tian, S.; Liu, K.; Ni, J.; Zhao, M.; Kang, Y.; Ma, X.; Guo, J. *Biosens. Bioelectron.* **2021**, *181*, 113160.

(26) Annavaram, V.; Chen, M.; Kutsanedzie, F. Y. H.; Agyekum, A. A.; Zareef, M.; Ahmad, W.; Hassan, M. M.; Huanhuan, L.; Chen, Q. *J. Photochem. Photobiol., A* **2019**, *382*, 111950.

(27) Wang, P.; Li, H.; Hassan, M. M.; Guo, Z.; Zhang, Z.-Z.; Chen, Q. *J. Agric. Food Chem.* **2019**, *67*, 4071−4079.

(28) Doughan, S.; Han, Y.; Uddayasankar, U.; Krull, U. J. *ACS Appl. Mater. Interfaces* **2014**, *6*, 14061−14068.

(29) Kim, K.; Jo, E.-J.; Lee, K. J.; Park, J.; Jung, G. Y.; Shin, Y.-B.; Lee, L. P.; Kim, M.-G. *Biosens. Bioelectron.* **2020**, *150*, 111885.

(30) Liu, Y.; Ouyang, Q.; Li, H.; Chen, M.; Zhang, Z.; Chen, Q. *J. Agric. Food Chem.* **2018**, *66*, 6188−6195.

(31) Bogdan, N.; Vetrone, F.; Ozin, G. A.; Capobianco, J. A. *Nano Lett.* **2011**, *11*, 835−840.

(32) Zhan, H.; Cheng, F.; Chen, Y.; Wong, K. W.; Mei, J.; Hui, D.; Lau, W. M.; Liu, Y. *Composites, Part B* **2016**, *84*, 222−227.

(33) Li, H.; Ahmad, W.; Rong, Y.; Chen, Q.; Zuo, M.; Ouyang, Q.; Guo, Z. *Food Control* **2020**, *107*, 106761.

(34) Liu, X.; Gao, T.; Gao, X.; Ma, T.; Tang, Y.; Zhu, L.; Li, J. *Microchim. Acta* **2017**, *184*, 3557−3563.

(35) Dong, H.; Sun, L.-D.; Yan, C.-H. *Chem. Soc. Rev.* **2015**, *44*, 1608−1634.

(36) Ouyang, Q.; Liu, Y.; Chen, Q.; Zhang, Z.; Zhao, J.; Guo, Z.; Gu, H. *Spectrochim. Acta, Part A* **2017**, *180*, 91−96.

(37) Muhr, V.; Würth, C.; Kraft, M.; Buchner, M.; Baeumner, A. J.; Resch-Genger, U.; Hirsch, T. *Anal. Chem.* **2017**, *89*, 4868−4874.